

A remarkably high fraction of strong Ly α emitters amongst luminous redshift $6.0 < z < 6.5$ Lyman break galaxies in the UKIDSS Ultra-Deep Survey

E. Curtis-Lake^{1*}, R. J. McLure¹, H. J. Pearce¹, J. S. Dunlop¹, M. Cirasuolo¹,
D. P. Stark^{2†}, O. Almaini³, E. J. Bradshaw³, R. Chuter³, S. Foucaud⁴,
W. G. Hartley³

¹ *SUPA†, Institute for Astronomy, University of Edinburgh, Royal Observatory, Edinburgh EH9 3HJ*

² *Department of Astronomy, Steward Observatory, University of Arizona, 933 North Cherry Avenue, Rm N204, Tucson, AZ, 8572*

³ *School of Physics & Astronomy, University of Nottingham, University Park, Nottingham NG7 2RD*

⁴ *Department of Earth Sciences, National Taiwan Normal University, No. 88, Section 4, T'ingzhou Road, Wenshan District, Taipei 11677, Taiwan*

24 October 2018

ABSTRACT

We present spectroscopic confirmation of ten highly luminous ($L \geq 2L^*$) Lyman alpha emitters in the redshift range $6.01 < z < 6.49$ (nine galaxies and one AGN), initially drawn from a sample of fourteen $z_{\text{phot}} \geq 6$ Lyman break galaxies (LBGs) selected from an area of 0.25 square degrees within the UKIDSS Ultra-deep Survey (UDS). Overall, our high rate of spectroscopic confirmation ($\geq 71\%$) and low rate of contamination provides a strong vindication of the photometric redshift analysis used to define the original sample. By considering star-formation rate estimates based on the Ly α and UV continuum luminosity we conclude that our sample is consistent with a Ly α escape fraction of $\simeq 25\%$. Moreover, after careful consideration of the potential uncertainties and biases, we find that 40%–50% of our sample of $L \geq 2L^*$ galaxies at $6.0 < z < 6.5$ display strong Ly α emission (rest-frame equivalent width $\geq 25\text{\AA}$), a fraction which is a factor of $\simeq 2$ higher than previously reported for $L \leq L^*$ galaxies at $z \simeq 6$. Our results suggest that, as the epoch of reionization is approached, it is plausible that the Ly α emitter fraction amongst luminous ($L \geq 2L^*$) LBGs shows a similarly sharp increase to that observed in their lower-luminosity ($L \leq L^*$) counterparts.

Key words: galaxies: high-redshift - galaxies: evolution - galaxies: formation

1 INTRODUCTION

Improving our understanding of the earliest epochs of galaxy formation and evolution relies fundamentally on the ability to select clean samples of high-redshift galaxies, free from significant low-redshift contamination. Traditionally, samples of high-redshift galaxies have been selected using one of two complementary photometric techniques. Firstly, Lyman-alpha emitters (LAEs) are selected from deep imaging using narrow-band filters centred on the redshifted Lyman-alpha emission line (e.g. Hu, Cowie & McMahon 1999). Alternatively, Lyman-break galaxies (LBGs) can be selected from deep broad-band photometry using the Lyman-break, or

“dropout”, technique pioneered by Steidel, Pettini & Hamilton (1995).

Studies of high-redshift galaxies selected using both techniques have made rapid progress recently, thanks to large-area, red-sensitive, detectors on ground-based telescopes and the ultra-deep near-infrared imaging now possible with WFC3/IR on-board the Hubble Space Telescope (HST). As a result, it is now possible to obtain large, statistical, samples of LBGs/LAEs in the redshift interval $6 < z < 7$ from the ground (e.g. Yoshida et al. 2006; Ouchi et al. 2008, 2010; McLure et al. 2009) and upwards of one hundred LBGs have now been identified in the redshift interval $6.5 < z < 8.5$ with WFC3/IR (e.g. Bouwens et al. 2010; McLure et al. 2010, 2011; Finkelstein et al. 2010). Indeed, recent results have demonstrated the power of these techniques with the spectroscopic confirmation of LBG-selected galaxies within the reionization epoch at $7.00 < z < 7.20$

* Email: efcl@roe.ac.uk

† Hubble Fellow

‡ Scottish Universities Physics Alliance

(Vanzella et al. 2011; Pentericci et al. 2011; Schenker et al. 2011; Ono et al. 2011). Although LAEs are simply a subset of the LBG population, due to the different selection techniques employed, the study of these two high-redshift galaxy populations has proceeded largely independently. As a consequence, one of the key questions in the study of high-redshift galaxies is determining how LAEs and LBGs are related and how they are connected to the galaxy populations identified at lower redshift.

Over the last fifteen years substantial observational effort has been invested in studying the population statistics of both LAEs and LBGs. As a result significant progress has been made towards an understanding of the luminosity function and clustering properties of the LAE and LBG populations from $z = 3$ to $z = 7$ (e.g. Bouwens et al. 2007, 2010, 2011; McLure et al. 2009, 2010; Ouchi et al. 2008, 2010; Reddy et al. 2008). While correlation length estimates for LAEs/LBGs are largely consistent ($r_0 \simeq 5$ Mpc) and show little evidence for evolution, the LAE/LBG luminosity functions appear to show substantial differential evolution. Most studies now agree that the LBG luminosity function evolves strongly with redshift, with L^* dimming by a factor of ≥ 2 between $z = 4$ and $z = 6$ (e.g. Bouwens et al. 2007; McLure et al. 2009, 2010; Yoshida et al. 2006). In contrast, the observed LAE luminosity function does not appear to evolve between $z = 3$ and $z = 6$ (e.g. Shimasaku et al. 2006; Ouchi et al. 2008), although the latest results indicate a moderate $\simeq 30\%$ drop in $L_{Ly\alpha}^*$ between $z = 5.7$ and $z = 6.6$ (Ouchi et al. 2010).

Studying the $Ly\alpha$ emission properties of LBG-selected samples is a powerful method for improving our understanding of this confusing picture (eg. Stark et al. 2010; Jiang et al. 2011). Although spectroscopic follow-up of the LBG population reveals $Ly\alpha$ emission in objects covering the full span of UV luminosity, the strongest $Ly\alpha$ emission (equivalent width $\gtrsim 100\text{\AA}$) is only observed in fainter objects. This was first indicated by Shapley et al. (2003), who observed the mean rest-frame $Ly\alpha$ equivalent width (EW) increasing at fainter magnitudes for $z \sim 3$ LBGs, and has since been noted by many authors over a wide redshift range (eg. Ando et al. 2006; Vanzella et al. 2009; Stark et al. 2010). Furthermore, studies of how the fraction of strong $Ly\alpha$ emitters evolves as a function of redshift offer the prospect of providing crucial information on the dust content of LBGs and, potentially, on the neutral fraction of the IGM. Recent work by Stark et al. (2010, 2011) has shown that, at fixed UV luminosity, the fraction of LBGs showing $Ly\alpha$ emission with $EW \geq 25\text{\AA}$ increases by 55% between $z = 4$ and $z = 6$. More recently this analysis has been extended to spectroscopically targeted $z \sim 7$ samples (Fontana et al. 2010; Schenker et al. 2011; Pentericci et al. 2011; Ono et al. 2011) with the results from different groups consistently showing a drop in the $Ly\alpha$ fraction at $z > 7$, tentatively attributed to a change in the neutral fraction in the IGM.

Recent theoretical studies find differing results when trying to explain the observed fractions of $Ly\alpha$ emitting galaxies amongst LBG samples. Dayal & Ferrara (2011) are able to broadly reproduce the observed trend of increasing $Ly\alpha$ emission with decreasing UV luminosity for an $EW > 55\text{\AA}$ cut at $z \sim 6$ from their cosmological SPH simulation of reionization. In agreement with recent observations, Dayal & Ferrara (2011) also find a decrease in the fraction of

strong $Ly\alpha$ emitters between $6 < z < 7$, though this is due mainly to changes in dust distributions, not a change in the neutral fraction of the IGM. However, they also conclude that all LBGs at $z \sim 6$ should display $Ly\alpha$ in emission with $EW > 20\text{\AA}$, in disagreement with the observations of Stark et al. (2011). Forero-Romero et al. (2011) are able to reproduce very well the observed fraction of $EW > 55\text{\AA}$ $Ly\alpha$ emitters in the $4.5 < z < 6.0$ sample from Stark et al. (2010), by requiring the escape fraction of $Ly\alpha$ photons to decrease with increasing UV-luminosity. In addition, they are also able to reproduce the observed drop in $EW > 25\text{\AA}$ $Ly\alpha$ emitters above $z > 6.3$ observed by Schenker et al. (2011), by fitting to the observed evolution in the LAE luminosity function at these redshifts. Neither of these studies allow for peculiar velocities (outflows/inflows) within the ISM which Dijkstra et al. (2011) find to produce a large effect on the detectability of $Ly\alpha$, with outflows from the galaxies boosting the observed EWs.

Despite the large amounts of effort invested in spectroscopically observing the properties of LBGs over recent years, one area of parameter space which has been relatively unexplored is that occupied by luminous LBGs at $z \geq 6$. The relatively poor statistics in this redshift-luminosity regime are simply a reflection of the relative rarity of $L \geq L^*$ galaxies at $z \geq 6$, combined with the small areas typically covered by survey fields with the deep, multi-wavelength, imaging necessary to reliably select such objects. In this paper we address this issue by presenting deep, red sensitive, optical spectroscopy of luminous ($L \geq 2L^*$) LBGs in the redshift interval $6.0 < z < 6.5$, photometrically selected from an area of 0.25 sq. degrees within the UKIDSS (Lawrence et al. 2007) Ultra-Deep Survey (UDS). Armed with deep spectroscopic observations, the combination of large area and deep optical/near-infrared imaging available in the UDS allows us to investigate three important issues. Firstly, we are able to investigate whether or not the photometrically selected LBG samples used to constrain the evolution of the bright end of the UV-selected galaxy luminosity function (e.g. McLure et al. 2009) are significantly contaminated by low-redshift interlopers and/or active galactic nuclei (AGN). Secondly, we are able to place the best available constraints on the fraction of strong $Ly\alpha$ emitters amongst luminous LBGs at $z \geq 6$. Finally, we are able to investigate whether previous reports of a very low fraction of strong $Ly\alpha$ emitters amongst samples of luminous $z \simeq 6$ LBGs have been biased due to contamination by low-redshift interlopers or small number statistics.

The structure of the paper is as follows. In Section 2 we describe the initial sample selection and spectroscopic observations before proceeding to present the spectra themselves. In Section 3 we describe our technique for accurately measuring the $Ly\alpha$ equivalent widths (EWs) and investigate the star-formation rates (SFRs) and $Ly\alpha$ photon escape fraction of our LBG sample, before estimating the fraction of luminous $z \simeq 6$ LBGs which are strong $Ly\alpha$ emitters. In Section 4 we compare our results to those from the recent literature and discuss the potential uncertainties and biases associated with estimating the $Ly\alpha$ emitter fraction at high redshift. In Section 5 we present our conclusions. Throughout the paper we assume a cosmology with $H_0 = 70 \text{ km s}^{-1} \text{ Mpc}^{-1}$, $\Omega_m = 0.3$, $\Omega_\Lambda = 0.7$. All magnitudes are quoted in the AB system (Oke & Gunn 1983).

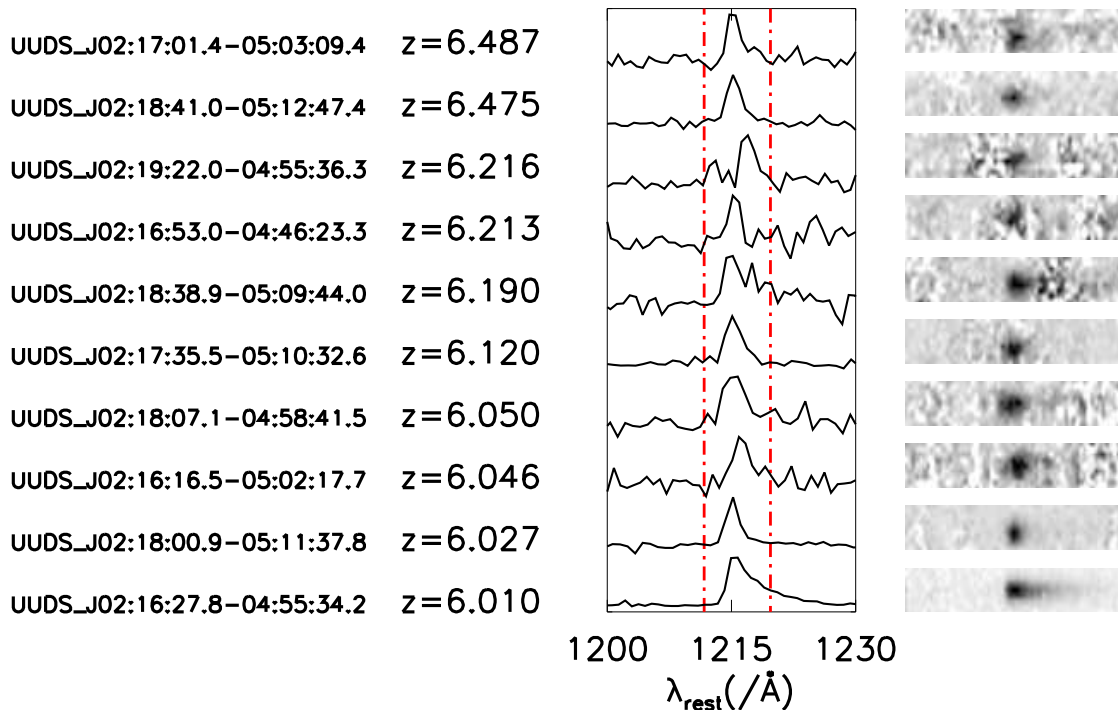


Figure 1. Spectra of the confirmed $z > 6$ objects showing the one-dimensional (1D) spectra to the left and the corresponding two-dimensional (2D) spectra on the right. All 1D spectra are plotted on the same flux scale, except for the spectrum of the AGN (UUJ021627.8) which has been scaled by a factor of 0.5.

2 IMAGING DATA, SAMPLE SELECTION AND SPECTROSCOPY

The sample of $z \geq 6$ LBG candidates targeted for spectroscopic follow-up is a sub-set of that originally selected by McLure et al. (2009), using photometric redshift analysis, to investigate the bright-end of the $z = 6$ galaxy luminosity function. Although a full description of the original selection process is provided in McLure et al. (2009), in this section we briefly review the most relevant details before proceeding to describe the spectroscopic observations.

2.1 Imaging data and LBG selection

The parent sample of $z \geq 6$ LBG candidates was originally selected via a photometric redshift analysis, which exploited the deep optical and near-infrared imaging available within the area covered by the UKIDSS Ultra-Deep Survey (UDS). The UDS is the deepest of the five near-infrared surveys being undertaken at the UK infra-red telescope (UKIRT) which together comprise the UK infra-red Deep Sky Surveys (UKIDSS; Lawrence et al. 2007).

The latest ESO-public data-release for the UDS (DR8) features near-infrared imaging over an area of 0.8 square degrees to 5σ -depths of $J = 24.9$, $H = 24.2$ & $K = 24.7$ ($2''$ diameter apertures). Within the UDS field, complimentary deep Subaru optical imaging is available from the Subaru/XMM Deep Survey (SXDS), which provides optical imaging to 5σ depths ($2''$ diameter apertures) of $B = 27.9$, $V = 27.3$, $R = 27.2$, $i' = 27.2$ & $z' = 26.1$ (Furusawa et al. 2008).

The useful overlap region between the UDS near-infrared and SXDS optical imaging covers an area of $\simeq 0.65$ square degrees, and it was from this overlap region that McLure et al. (2009) used a photometric redshift analysis to select luminous ($z' < 26$) LBG candidates in the redshift interval $4.5 < z < 6.5$. The original selection utilised the full information available from the SXDS optical bands and the UKIDSS DR1 J - and K -band near-infrared imaging. Our updated photometric redshift analysis, using the UKIDSS DR8 J , H and K -band imaging, is described in greater detail in Section 2.2.3. The parent sample for spectroscopic follow-up was comprised of those candidates with a high probability of lying at $z \geq 6$ based on the redshift probability density function returned by the photometric redshift analysis.

2.2 Spectroscopy

The spectroscopic data analysed in this study were obtained between October 2007 and January 2011 with the FORS2 spectrograph on the VLT as part of the systematic spectroscopic follow-up of the UDS obtained through the ESO large programme ESO 180.A-0776 (UDSz; P.I. O. Almaini). Given that full details of UDSz will be presented in Almaini et al. (2012, in preparation), only the most relevant details are provided here.

The UDSz programme was allocated a total of 235 hours of observations, with 93 hours allocated for observations with the VIMOS spectrograph and 142 hours allocated for FORS2 observations. The primary science driver for UDSz was to obtain spectroscopic observations of a representative

Table 1. The spectroscopic sample of $z \geq 6$ UDS LBGs. Column 1 lists the UDS object IDs (incorporating the J2000 coordinates). Column 2 gives the spectroscopic redshift and errors derived from the FORS2 spectra, taking the spectroscopic redshift from the peak of the Ly α line. Columns 3 & 4 give the quality of the spectroscopic redshift (A–C, see text for details) and the photometric redshift derived in Section 2.3 respectively. The remaining columns list the z' -band and z_{921} -NB observed magnitudes (corrected to total) plus errors, absolute UV magnitude derived from the z_{921} -NB photometry and the measured Ly α fluxes and EWs (derived from spectra, see text for more details).

ID	z_{spec}	Quality	z_{phot}	m_z	m_{912}	M_{UV}	Ly α flux ($/10^{-18}$ ergs s $^{-1}$ cm $^{-2}$)	Ly α EW (\AA)
UUDS_J021800.90-051137.8	6.027 ± 0.002	A	$6.0^{+0.1}_{-0.1}$	25.36 ± 0.08	25.30 ± 0.09	-21.40	44.9 ± 7.4	54.7 ± 11.3
UUDS_J021616.53-050217.7	6.046 ± 0.004	A	$5.9^{+0.2}_{-0.1}$	25.35 ± 0.15	25.84 ± 0.13	-20.86	17.8 ± 3.1^a	36.8 ± 8.5
UUDS_J021807.14-045841.5	6.050 ± 0.003	A	$6.0^{+0.2}_{-0.1}$	25.02 ± 0.12	24.99 ± 0.10	-21.72	29.4 ± 2.6	27.6 ± 4.1
UUDS_J021816.33-051116.6	6.114 ± 0.009	C	$6.1^{+0.3}_{-0.3}$	25.55 ± 0.15	25.42 ± 0.14	-21.29	7.3 ± 1.7	11.6 ± 3.1
UUDS_J021735.34-051032.6	6.120 ± 0.003	A	$6.0^{+0.1}_{-0.1}$	25.21 ± 0.12	25.47 ± 0.15	-21.25	31.4 ± 2.6	46.8 ± 8.4
UUDS_J021838.90-050944.0	6.190 ± 0.014	A	$6.0^{+0.2}_{-0.1}$	25.21 ± 0.11	25.13 ± 0.11	-21.62	36.4 ± 3.4	39.4 ± 6.0
UUDS_J021653.00-044623.3	6.213 ± 0.004	A	$6.5^{+0.4}_{-0.4}$	25.75 ± 0.21	25.34 ± 0.09	-21.41	9.5 ± 1.1	12.5 ± 3.1
UUDS_J021922.01-045536.3	6.216 ± 0.009	A	$6.4^{+0.8}_{-0.8}$	25.79 ± 0.22	26.25 ± 0.20	-20.50	16.8 ± 2.2	50.7 ± 12.8
UUDS_J021841.02-051247.4	6.475 ± 0.003	A	$5.9^{+0.4}_{-0.2}$	25.80 ± 0.23	25.46 ± 0.16	-21.36	18.2 ± 3.1^a	27.8 ± 6.8^b
UUDS_J021701.44-050309.4	6.487 ± 0.004	A	$6.0^{+0.3}_{-0.3}$	25.91 ± 0.19	25.03 ± 0.10	-21.79	10.2 ± 1.8^a	10.6 ± 2.3^b

^a Ly α flux calibration tied to the z -band photometry using an average correction factor, see text for details.

^b EW values potentially affected by Ly α contributing to the NB photometry used to derive the UV continuum value.

sample of K -band selected galaxies ($K < 23$) photometrically pre-selected to lie at redshift $z_{phot} \geq 1.0$. These spectroscopic observations were designed to support the primary science driver of the UDS survey, which is to study the assembly and evolution of massive galaxies at $z \geq 1$. Within this context, the large allocation of FORS2 time (20 MXU masks, 5 hours of integration each) was designed to provide sensitive, red optical, spectra of massive galaxies in the redshift interval $1.0 < z < 1.5$.

Each of the 20 FORS2 masks covers an area of $6.8' \times 6.8'$ and typically allowed for the allocation of 30–35 science slits (based on a slit length of $8''$). During the mask design process targets from the core sample of $K < 23$ galaxies were allocated with the highest priority. However, in order to fill each mask, several other samples of additional science targets were also allocated slits on a best-effort basis. The list of high-redshift LBG candidates from McLure et al. (2009) with a high probability of lying at $z \geq 6$ was included as one of the samples of additional science targets. A total of fourteen $z \geq 6$ LBG candidates were observed as part of UDSz, each receiving a total of 5-hours of on-source integration with the GRS.300I grism ($6000\text{\AA} < \lambda < 10000\text{\AA}$ with $R = 660$). Data reduction was performed using a modified version of the FORS2 pipeline, details of which are provided in Pearce et al. (2011, in preparation).

2.2.1 Spectra of confirmed $z \geq 6$ sources

Of the fourteen galaxies for which spectra were obtained we are able to assign secure redshifts to eleven sources according to Ly α line detections, placing them at $z > 6$. The 1D spectra for the spectroscopically confirmed $z > 6$ Ly α emitters are displayed in Figure 1 and the measured line fluxes and EWs are reported in Table 1. Many of the spectra show continuum red-wards of the emission line as well as the distinctive asymmetrical line profile indicative of Ly α . Each redshift is assigned a quality flag, defined as in Vanzella et al. (2009), with values of A (unambiguous detection), B (likely detection) and C (uncertain detection). It should be noted that the redshifts for the 11 confirmed $z > 6$ sources

are measured from the position of peak flux within the Ly α line, and are hence susceptible to shifts in the peak position due any velocity structure of the neutral hydrogen within the galaxy or the surrounding IGM. The average velocity shift measured for Ly α in lower redshift samples is of order $+350$ km s $^{-1}$ (Adelberger et al. 2003; Shapley et al. 2003), since the Ly α photons are more likely to escape the galaxy when they are scattered off neutral Hydrogen that is travelling away from us, giving the photons a Doppler shift that takes them off resonance.

One of our targets (UUDS_J021627.80-045534.2) is a low-luminosity active galactic nucleus (AGN) at a redshift of $z = 6.01$ (Ly α FWHM $\simeq 1600$ km s $^{-1}$). This object was initially identified as a potential ultra-luminous $z \simeq 6$ LBG candidate by McLure et al. (2006) and was subsequently targeted as a high-redshift quasar candidate by Willott et al. (2009). In Willott et al. (2009) this source is referred to as CFHQS J021627–045534, and was confirmed as a low-luminosity quasar at $z = 6.01$ based on a four-hour spectrum obtained with the GMOS spectrograph on Gemini. However, it is important to note that CFHQS J021627–045534 was the only $z \simeq 6$ AGN identified by Willott et al. (2010) over a search area of 4.47 sq. degrees, down to a limit of $z' = 24.5$. Based on this fact, and the steepness of the $z \simeq 6$ UV-selected galaxy luminosity function, it seems reasonable to conclude that the luminous, type I AGN contamination of $26 \geq z' \geq 25$ LBG samples at $z \simeq 6$ is negligible.

Based on the optical spectra alone, we cannot entirely rule out the possibility that the observed Ly α emission could have some contribution from a narrow-line AGN component. However, we note that a recent study of UV-selected AGN at $z \sim 2 - 3$ by Hainline et al. (2011) indicates that narrow-line AGN are on average much redder than non-AGN LBGs ($\beta = -0.314$ compared to $\beta = -1.49$) and show the NV line at $\lambda_{rest} = 1240\text{\AA}$ in emission. Given that our sample have broad-band SEDs which are not well reproduced by a standard Type-2 AGN template (see Figure 2), are not detected at $24\mu\text{m}$ and do not display NV emission lines in their FORS2 spectra, we conclude that the UV continuum in these objects is dominated by starlight.

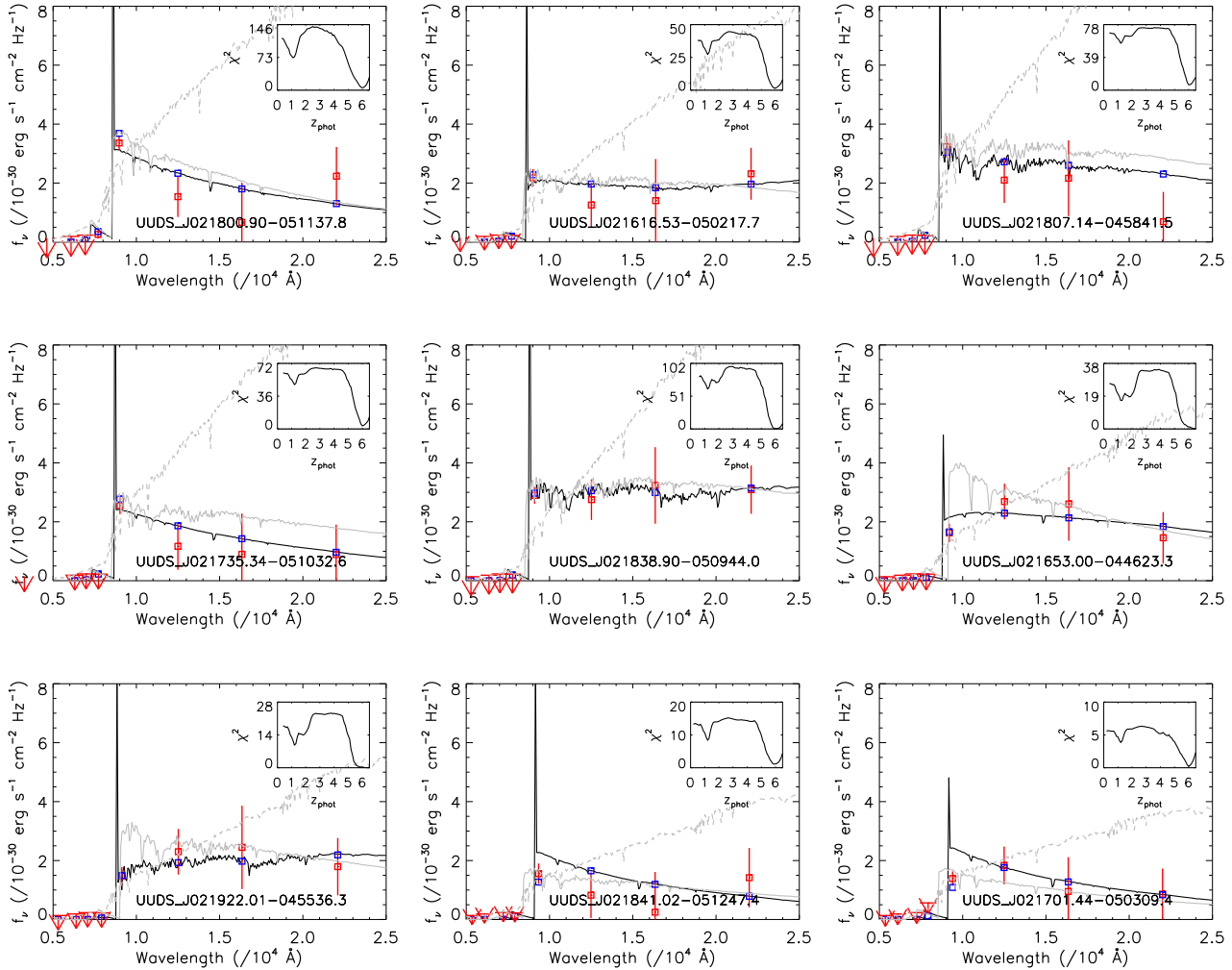


Figure 2. SED fits to the spectroscopically confirmed $z \geq 6$ LBGs showing the *BVRizJHK* photometry (red data points with error bars), the best fitting template with a fixed spectroscopic redshift and including the measured Ly α contribution (black line and blue data points) and the best-fitting template assuming no Ly α flux and leaving redshift as a free parameter (grey lines). The best-fitting SED templates at low redshift ($z_{\text{phot}} \leq 2$) are plotted as dashed grey lines. The inset panels show the distribution of χ^2 versus redshift.

2.2.2 Spectra of unconfirmed sources

Four of the $z \geq 6$ LBG candidates which were spectroscopically observed did not produce spectra which allow us to assign a robust redshift. One of these four objects (UUDS_J021816.33-051116.6) does display a probable Ly α emission line but is assigned a quality flag of C since the emission line sits within a region of poorly subtracted sky-line residuals. One further object does not display a prominent Ly α emission line, but does display a continuum break consistent with a redshift of $z = 5.83$. However, the signal-to-noise in the final FORS2 spectrum is too low to be confident of the redshift.

The spectra of the remaining two candidates show only a very faint continuum, with a signal-to-noise ratio too low to reliably distinguish between a Lyman break and low-redshift interloper. We note that three of the four unconfirmed candidates lie on the same FORS2 mask. However, although this mask is slightly poorer than average, in terms of redshift completeness for primary targets at $1 < z < 1.5$,

there is no particular reason to suspect that the spectra of these three high-redshift candidates have been unduly affected.

2.3 Photometric redshift selection and spectroscopic completeness

From the sample of fourteen $z \geq 6$ LBG candidates which were selected for spectroscopic follow-up, a total of ten objects have been robustly spectroscopically confirmed as $z \geq 6$ objects. As a consequence, regarding the other four spectra as contaminants, the lower limit to the spectroscopic completeness for our sample is 71%. However, as described above, two of the remaining spectra display strong evidence of being genuine high-redshift galaxies at $z \geq 5.8$ and have only failed to make our robust sample due to insufficient signal-to-noise. If we regard these two objects as also being confirmed $z \simeq 6$ objects, then the spectroscopic completeness of our sample rises to 86%. Irrespective of the na-

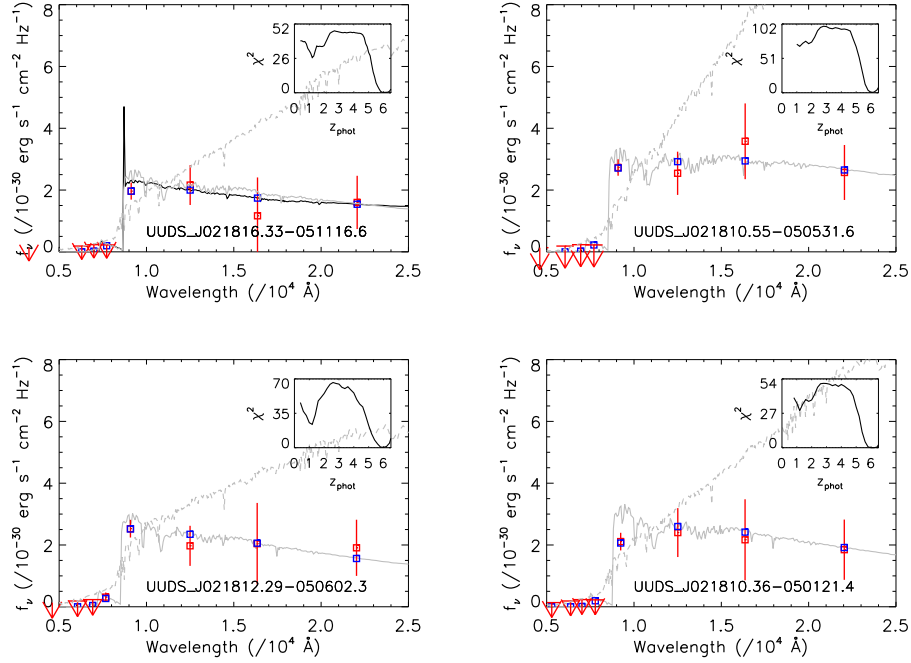


Figure 3. SED fits for the three unconfirmed objects and UUDS_J021816.33-051116.6, which is assigned a quality ‘C’ emission line redshift (see text) and is not treated as a secure Ly α detection. For the three objects without an assigned spectroscopic redshift, only the primary and secondary photometric redshift solutions are shown as grey solid and dashed lines respectively. For these objects the model fluxes are calculated from the primary redshift solution (blue points).

ture of the two uncertain candidates, the high spectroscopic completeness provides a strong vindication of the original method of selecting high-redshift targets on the basis of an SED-fitting photometric redshift analysis.

To illustrate this point, in Fig. 2 we show the latest photometry available for each of the spectroscopically targeted $z \geq 6$ objects, along with the results of our updated photometric redshift analysis. For each object the observed photometry is plotted along with the best-fitting SED model returned when redshift is kept as a free parameter, as well as the best-fitting model using the fixed spectroscopic redshift and adding a Ly α emission line with the correct EW. The photometric redshifts were calculated using LePhare photometric redshift code (Ilbert et al. 2006). The galaxy templates were made using the Bruzual & Charlot (2003) stellar population synthesis models, with exponentially decreasing star formation rates with e -folding times in the range $0.1 \text{ Gyr} < \tau < 30 \text{ Gyr}$ and a Chabrier (2003) initial mass function (IMF). Reddening by dust is added using the Calzetti et al. (2000) extinction law with $E(B-V)$ values ranging from 0.0 to 0.5. For the fitting with fixed redshift, Ly α is added to the models after extinction is applied, using the flux from the template convolved with the narrow-band filter as the estimate of the continuum to translate the EW into the Ly α flux.

In Fig. 3 the insets showing the distribution of χ^2 versus photometric redshift clearly demonstrate, as expected, that the primary photometric redshift solutions are all at $z \geq 6$. Crucially, it can also be seen that any competing low-redshift solution (shown as the dashed grey SED fits) can be ruled-out at high statistical significance. The fundamental reason for this is the additional information on the spectral slope

long-ward of Ly α provided by the UDS near-infrared photometry. Without this additional information any sample of bright $z \simeq 6$ LBGs candidates is vulnerable to substantial contamination by low-redshift interlopers, a point we will return to in Section 4.

3 LYMAN ALPHA

3.1 Ly α equivalent widths

The Ly α equivalent widths were obtained by measuring the observed line flux, and estimating the UV continuum at Ly α from Subaru NB921 narrow-band (NB) imaging available in the UDS (Sobral et al. 2011).

The line flux was measured by subtracting any continuum from the line profile, where the continuum is estimated from regions either side of the line unaffected by sky line residuals, then integrating the flux over the pixels contributing to the line. To ensure that the calibration of the spectra matches the photometry, they are convolved with the Subaru z' -band filter profile and the flux scaled to match the z' -band photometry (see Fig. 4). To ensure that sky residuals do not dominate the derived flux from the convolved spectrum, the continuum level is estimated just red-wards and blue-wards of Ly α and is modelled by a simple step function. Over the small wavelength range within the filter, differences in true slope red-wards of Ly α produce minimal differences to the final convolved flux.

Absolute calibration of the spectra in this way is not effective if the signal-to-noise is so low in the continuum that it is effectively measured as zero. In these cases (noted in

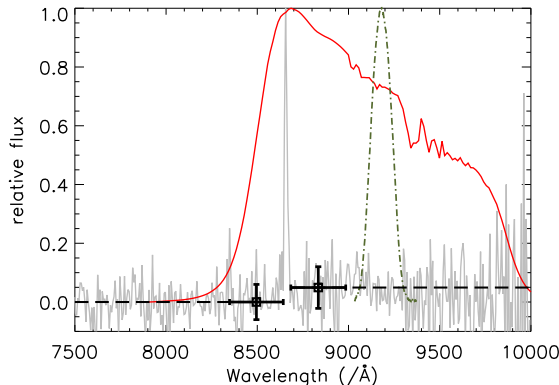


Figure 4. An illustration of the method adopted to calculate the Ly α EWs. The spectrum is of object UUDSJ.021735.34-051032.6 scaled to the height of the Ly α line. Over-plotted as the red solid line is the throughput of the Subaru z' -band filter. The spectrum is convolved with this filter and scaled to match the z' -band photometry. To ensure that sky residuals do not dominate the convolution the continuum is modelled as a simple step function, as shown by the black long dashed line, where the continuum is derived from regions either side of the emission lines (shown by the points with associated error bars). The green dot-dashed line shows the Subaru narrow-band NB921 filter profile. Photometry from this filter is used to determine the rest-frame UV flux redward of Ly α emission. This is used with the calibrated line flux to determine the Ly α EW.

Table 1) the median correction factor measured from all the other spectra is used and the standard deviation of correction factors is folded into the final error for these line fluxes.

The final error in the Ly α flux measurement includes pixel error estimates from the noise array, estimated error in the subtracted continuum measurement, as well as the estimated error in the derived calibration. This calibration error includes the error in the convolved flux, assuming errors per pixel derived from the standard deviation of pixel values for those contributing to continuum estimates, as well as the errors in the z' -band photometry.

The NB921 photometry samples the continuum redwards of Ly α for $z < 6.5$ (see Fig. 4) and to estimate the continuum at Ly α a flat UV continuum in F_ν ($F_\lambda \propto \lambda^{-2}$) is assumed. The NB photometry is used to estimate the UV continuum rather than direct measurements made from the spectra because sky subtraction hinders accurate continuum measurements in the spectra, as well as the signal-to-noise in any detected continuum being very low (< 2) in many of the spectra. The errors in the derived EWs include the errors in NB photometry³. No attempt was made to correct either the UV continuum or Ly α line flux for dust extinction during the EW calculation.

³ For the two highest redshift LBGs, the Ly α emission line lies within the extreme blue-end of the NB921 filter. Although the throughput of the filter is extremely low at these wavelengths, it is possible that the resulting EW measurements are underestimated by $\lesssim 5\%$.

Table 2. Star-formation rates derived from Ly α emission-line luminosity and UV continuum luminosity (without any correction for dust extinction). The UV-derived SFR (SFR_{UV}) is estimated from the UV luminosity at $\lambda_{rest} = 1500\text{\AA}$ using equation 1 and the Ly α -derived SFR ($SFR_{Ly\alpha}$) is estimated from the luminosity of the Ly α emission using equation 2.

ID	$SFR_{Ly\alpha}$ ($/M_\odot \text{ yr}^{-1}$)	SFR_{UV} ($/M_\odot \text{ yr}^{-1}$)
UUDSJ021800.90-051137.8	13.8 ± 1.3	30.2 ± 2.6
UUDSJ021616.53-050217.7	7.4 ± 1.3	18.4 ± 1.7
UUDSJ021807.14-045841.5	12.3 ± 1.1	40.6 ± 3.8
UUDSJ021735.33-051032.6	13.4 ± 1.1	26.3 ± 3.6
UUDSJ021838.90-050944.0	16.0 ± 1.5	37.0 ± 3.8
UUDSJ021653.00-044623.3	4.2 ± 0.5	30.5 ± 2.4
UUDSJ021922.01-045536.3	7.5 ± 1.0	13.2 ± 2.4
UUDSJ021841.02-051247.4	8.8 ± 1.5	29.1 ± 4.4
UUDSJ021701.44-050309.4	5.0 ± 0.9	43.3 ± 4.0

Both the z' -band and narrow-band fluxes were corrected to total using measured aperture corrections from stars within the individual SXDS pointings. The measured equivalent widths were compared to estimates taken directly from the spectra themselves and are found to be in good agreement, indicating that the quoted equivalent widths are secure.

3.2 Ly α and UV-derived SFRs

Both the UV continuum and Ly α emission-line luminosity are commonly used to derive SFR estimates. Both of these indicators are sensitive to the presence of dust and Ly α is also sensitive to neutral hydrogen within the galaxy and the surrounding IGM. In Fig. 5 we compare the SFR estimates derived from the UV continuum luminosity using the Madau et al. (1998) formula (corrected to a Chabrier IMF), with those derived from the measured Ly α luminosity (e.g. Nilsson et al. 2009), with no correction for dust extinction:

$$L_{UV} \text{ (ergs}^{-1}\text{Hz}^{-1}\text{)} = 4.8 \times 10^{27} \times SFR_{UV} \text{ (}/M_\odot\text{yr}^{-1}\text{)} \quad (1)$$

$$L_{Ly\alpha} \text{ (ergs}^{-1}\text{)} = 9.7 \times 10^{41} \times SFR_{Ly\alpha} \text{ (}/M_\odot\text{yr}^{-1}\text{)} \quad (2)$$

The constant in equation 2 is based on the continuum luminosity at $\lambda_{rest} = 1500\text{\AA}$ and has been converted to a Chabrier IMF using a ratio of 1.65, the asymptotic ratio between the number of ionizing photons produced by a constant SFR with a Salpeter compared to a Chabrier IMF predicted by Bruzual & Charlot (2003).

Although there is a large scatter between the two SFR measurements, it can immediately be seen from Fig. 5 that the SFR estimate provided by the Ly α luminosity is systematically lower than that provided by the UV continuum luminosity, with a mean value of $SFR_{Ly\alpha}/SFR_{UV} = 0.36 \pm 0.05$, and a median of 0.4.

We note that this is very close to the value of 0.4 which would be predicted by the recent study of the redshift evolution of the Ly α escape fraction by Hayes et al. (2011). At low redshift Hayes et al. (2011) calculate $f_{esc}^{Ly\alpha}$ by comparing the observed Ly α luminosity function with a prediction based on the extinction corrected H α luminosity function (assuming case B recombination). The lack of observed H α

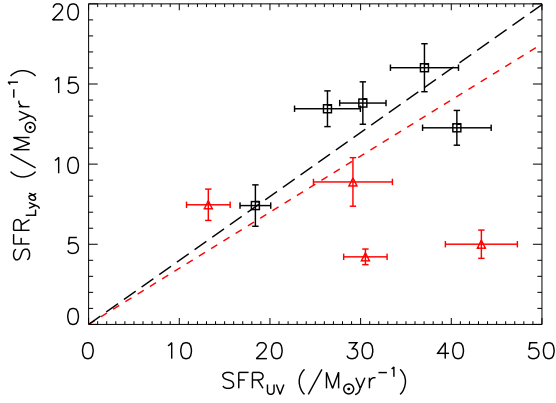


Figure 5. Ly α -derived SFRs vs. UV-derived SFRs. The short dashed red line shows the mean Ly α :UV SFR ratio (0.36) and the black long dashed line shows the ratio of 0.4 predicted from Hayes et al. (2011) (for $f_{esc}^{Ly\alpha} = 0.25$ at $z \sim 6$). Objects with $z > 6.2$ are plotted as red triangles.

luminosity functions above $z \sim 2.3$, means that at higher redshifts, the intrinsic Ly α luminosity function is predicted from the UV, with extinction estimates being made from SED fitting. This calculation is essentially taking the ratio of the Ly α and UV star formation rate densities, $\dot{\rho}_\star$ (equations 3-5), where the star-formation rate densities are derived from integrating over the Ly α and UV luminosity functions respectively, i.e.

$$f_{esc}^{Ly\alpha} = C_1 \left(\frac{\dot{\rho}_\star^{Obs} Ly\alpha}{\dot{\rho}_\star^{Obs} UV} \right)^{1+C_2} \quad (3)$$

$$C_1 = C_{Ly\alpha}^{-C_2} \quad (4)$$

$$C_2 = \frac{k_{UV}}{k_{Ly\alpha} - k_{UV}} \quad (5)$$

Where $k_{UV} = 10.3$ (Calzetti et al. 2000) and $k_{Ly\alpha} = 13.8$ and $C_{Ly\alpha} = 0.445$ are derived from a fit to the observed anti-correlation between E_{B-V} and f_{esc} . Based on this formalism, Hayes et al. (2011) find that the escape fraction varies as $f_{esc}^{Ly\alpha} \propto (1+z)^\xi$ with $\xi = 2.57^{+0.19}_{-0.12}$, giving $f_{esc}^{Ly\alpha} \simeq 0.25$ at $z \simeq 6$, hence providing an estimate of $SFR_{Ly\alpha}/SFR_{UV} \sim 0.4$, which agrees with the mean value derived here, within the errors. Consequently, based on the results of Hayes et al. (2011), we conclude that our sample of $L \geq 2L^*$ LBGs at $z \simeq 6$ are consistent with a Ly α escape fraction of $f_{esc}^{Ly\alpha} \simeq 25\%$.

Finally, we note that in Fig. 5, while most of the sample agree well with the prediction of Hayes et al. (2011), the two largest outliers are drawn from the high-redshift end of the sample at $z > 6.2$ and suggest a lower value of $f_{esc}^{Ly\alpha}$.

4 THE LYMAN-ALPHA EMITTER FRACTION

In this section we use our sample of spectroscopically confirmed LBGs to provide entirely new information on the Ly α

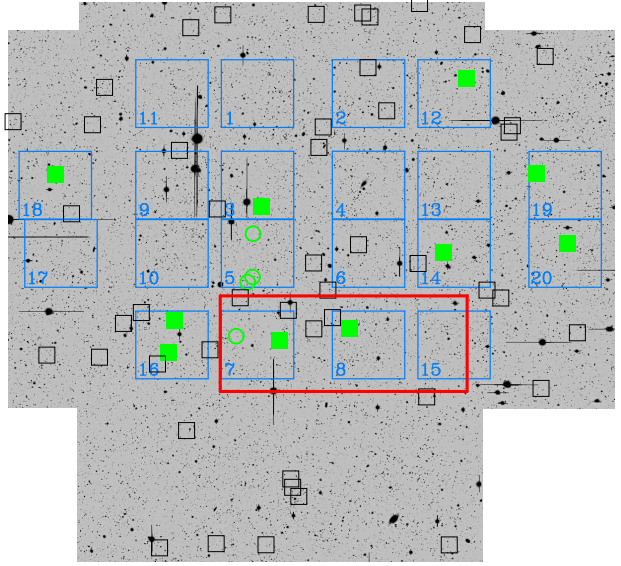


Figure 6. A greyscale representation of the region with overlapping Subaru (optical) and UKIRT (near-infrared) data in the UDS. Over-plotted in blue are the locations of the 20 FORS2 masks from the UDSz programme and the area imaged by HST/WFC3 as part of the CANDELS survey (Grogin et al. 2011) is shown in red. The small black squares show all the objects in the field that are plausible $z \geq 6$ candidates following the criteria described in the text. The green squares show the spectroscopically confirmed $z \geq 6$ LAEs, while the green circles show the objects for which the FORS2 spectra do not provide an unambiguous redshift.

emitter fraction of $L \geq 2L^*$ LBGs at $z \geq 6$. As previously described, the original sample of spectroscopic candidates was selected using the redshift probability density function derived using a photometric redshift analysis (McLure et al. 2009). However, although this strategy makes optimal use of the available data, in order to perform a comparison between our results and those in the literature it is necessary to re-engineer our candidate selection in terms of traditional colour-cut criteria. Consequently, all of the parent sample considered for spectroscopic follow-up also satisfy the following criteria:

$$z' < 26 \quad (6)$$

$$i' - z' \geq 2.0 \quad (7)$$

$$z' - J \leq 0.8 \quad (8)$$

where all magnitudes are measured within a $2''$ diameter aperture and we also require each object to be a non-detection in the BVR bands at the 2σ level. The choice of a stringent $i' - z' \geq 2$ colour cut is motivated by the fact that any galaxy at $z \geq 6$ is predicted to display a drop of at least two magnitudes between the Subaru i' and z' filters assuming the Madau (1995) prescription for IGM absorption. The $z' - J \leq 0.8$ colour-cut is motivated by the desire to effectively exclude low-redshift interlopers at $z \simeq 1.5$, while maintaining sensitivity to genuine $z \geq 6$ galaxies with moderate reddening.

Within the overlap region between the optical and near-infrared imaging in the UDS the surface density of objects obeying the above selection criteria is 0.023 ± 0.003 per

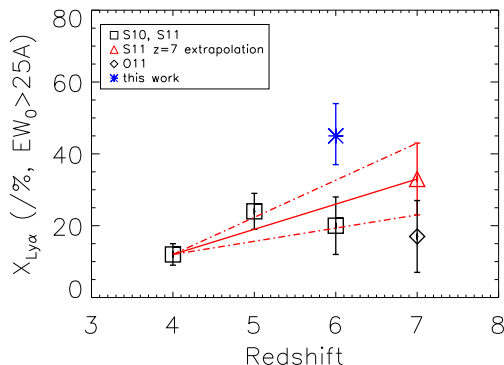


Figure 7. The evolution with redshift of the fraction of luminous LBGs ($-21.75 < M_{UV} < -20.25$) which display $\text{Ly}\alpha$ line emission with rest-frame $\text{EW} \geq 25\text{\AA}$. The black squares show the measured fractions from Stark et al. (2010, 2011) and the black diamond is the measured fraction at $z \sim 7$ estimated by Ono et al. (2011) from the combination of a number of spectroscopic samples. The red triangle shows the expected value at $z \sim 7$ extrapolated from the trends at lower redshift (Stark et al. 2011), with the fitted linear relationship and uncertainties plotted as the red solid and dashed lines, respectively. The blue star shows the results of this work based on the sample selected from the UV-continuum flux and with upper and lower limits as described in the text.

square arcmin. Therefore, within the total area covered by the FORS2 pointings (20 pointings, each covering an area of $6.8' \times 6.8'$), we would expect $\sim 15 - 20$ candidates. From Fig. 6, which shows the region of optical/near-infrared overlap in the UDS with the positions of the FORS2 masks and the candidates satisfying the above criteria over-plotted, it can be seen that there are 19 candidates in this area, with 14 of those having been targeted for spectroscopy. Consequently, we conclude that the sample of candidates targeted for spectroscopy appears to be consistent with being drawn randomly from the parent population of candidates satisfying the colour-cut criteria described above (although see section 4.2.4 for further discussion).

From our sample of fourteen objects we find seven which display strong $\text{Ly}\alpha$ emission ($\text{EW} \geq 25\text{\AA}$), which suggests a minimum $\text{Ly}\alpha$ emitter fraction of 50%. However, if we exclude the AGN from our sample this fraction increases to 54%. Either way, these are very high $\text{Ly}\alpha$ fractions compared to previous literature results for luminous LBGs and clearly require some discussion.

4.1 Comparison with the literature

We now look to other studies of spectroscopically targeted LBGs at $z \sim 6$ to see whether this $\text{Ly}\alpha$ fraction is comparable. Stark et al. (2011) present a sample of i' -band dropouts selected with a $i'_{775} - z_{850} > 1.3^4$ colour cut, which is a considerably bluer cut than that adopted here.

⁴ i'_{775} and z_{850} are the F775W and F850LP HST/ACS filters respectively.

This sample, when compared to results at lower redshift (Stark et al. 2010), provides strong evidence that the fraction of objects showing $\text{Ly}\alpha$ in emission increases from $z = 4$ to $z = 6$ for galaxies in the absolute magnitude range $-20.25 < M_{UV} < -18.75$. However, in contrast, little evolution in the $\text{Ly}\alpha$ fraction is seen for brighter objects with UV luminosities more comparable to our sample ($-21.75 < M_{UV} < -20.25$). In this luminosity range, Stark et al. (2011) find that the fraction of objects showing $\text{Ly}\alpha$ in emission is $20\% \pm 8.1\%$ and $7.4\% \pm 5.0\%$ for objects with EWs greater than 25\AA and 55\AA respectively.

Considering the small size of our sample, at the higher $\text{EW} \geq 55\text{\AA}$ threshold our results are in reasonably good agreement with Stark et al. (2011), given that one of our objects has $\text{EW} \simeq 55\text{\AA}$ (i.e. 1/9). However, at the lower $\text{EW} \geq 25\text{\AA}$ threshold our sample shows a substantially larger fraction of LBGs with $\text{Ly}\alpha$ emission ($\simeq 54\%$).

4.2 Potential biases

Understanding or reconciling the difference in the measurements made by these two studies is difficult due to the different selection mechanisms used and the small numbers of bright objects available for study in fields smaller than the UDS. In fact, it is not clear that a direct comparison between our results and those of Stark et al. (2011) is actually meaningful, given that the vast majority of our sample are confined to the bright half of the luminous absolute magnitude bin ($-21.75 < M_{UV} < -20.25$) defined by Stark et al. (2011). However, given that the trend reported by Stark et al. (2011), is for a *decreasing* fraction of strong $\text{Ly}\alpha$ emitters at $z \simeq 6$ with increasing UV luminosity, our results indicating a high fraction of $\text{Ly}\alpha$ emitters amongst luminous $z \geq 6$ LBGs clearly requires some explanation. In this section we investigate several effects which could have potentially biased our determination of the $\text{Ly}\alpha$ emitter fraction.

4.2.1 Reddening

First, we consider whether our colour selection criteria are selecting against galaxies with internal reddening by dust that may produce lower $\text{Ly}\alpha$ EWs. The $i' - z' \geq 2.0$ colour cut does not select against reddened galaxies as this colour is dependent on the fraction of flux attenuated in clumpy HI regions in the intervening IGM, which is independent of the galaxy properties. Reddening tends to increase this colour since there is more flux at redder wavelengths still contributing to the z' -band flux. It is possible that the true IGM absorption for individual galaxies may scatter the colours of genuine $z \geq 6$ galaxies below the colour cut, but this scatter should be independent of the intrinsic galaxy properties. The $z' - J$ colour cut may well exclude a few redder $z \geq 6$ galaxies from our sample. This colour cut is designed to exclude low-redshift galaxies and cool galactic stars which are able to satisfy the $i' - z'$ colour cut. However, because we are insisting on a strict $i' - z' \geq 2.0$ colour, only five additional objects are excluded on the basis of the $z' - J \leq 0.8$ criterion over the entire UDS field, so we do not expect our sample to be greatly biased towards dust-free galaxies.

However, it is important to note that if a bluer $i' - z'$ colour cut is adopted, the potential for contamination increases due to a population of massive red galaxies at

$z \simeq 1.5$ with a surface density which increases significantly at $z' \leq 26$. As a result, any samples selected without near-infrared data and a bluer $i' - z'$ colour cut will be significantly contaminated by low-redshift interlopers at $z' \leq 26$. Of course, until the present study, selecting significant samples of $z \simeq 6$ objects with $z' \leq 26$ has not been possible due to insufficient area.

4.2.2 Contamination from low-redshift interlopers

To further explore how low-redshift interlopers could contaminate samples of bright $z \simeq 6$ LBGs, we have investigated different selection criteria using the deep HST data available in GOODS-S. All of our objects were found to satisfy the HST colour selection of $i_{775} - z_{850} > 1.7$. This lower colour cut is due to the difference in filter profiles between the HST z_{850} -band compared to the Subaru z' band, as well as slightly increased overlap between the HST i_{775} and z_{850} band filters. With the new HST/WFC3 near-infrared data available as part of the CANDELS survey (Grogin et al. 2011; Koekemoer et al. 2011) we can investigate how our $z' - J$ cut may affect these samples. We find that only two objects in the field satisfy $i_{775} - z_{850} > 1.7$ with $z_{850} < 26$, both of which are excluded by a $z_{850} - J_{125} < 0.75$ criterion (consistent with our $z' - J < 0.8$ colour cut). However, in a sample selected using $i_{775} - z_{850} > 1.3$; $z_{850} < 27$, we find that $> 90\%$ of objects survive the $z_{850} - J_{125} < 0.75$ colour cut. It is therefore clear that while a colour-cut of $i_{775} - z_{850} > 1.3$ should be sufficient to select a clean sample of $z \simeq 6$ LBGs at $z_{850} \simeq 27$, at magnitudes brighter than $z' \leq 26$ suitably deep near-infrared photometry is essential to avoid significant contamination from low-redshift interlopers. In fact, this point is very well illustrated by the SED template fits to our spectroscopically confirmed LBGs shown in Fig. 2.

4.2.3 EW measurements and cosmic variance

It is worth noting at this point that two of our objects with strong Ly α emission have EWs that are quite close to the $\text{EW} \geq 25\text{\AA}$ cut. Although our method of EW calculation is quite robust, not all fields have narrow band imaging just red-wards of Ly α to supply a continuum estimate, and it is difficult to get high signal to noise in the continuum from the actual spectra at these redshifts. It is certainly feasible that with a different continuum estimator, or a lower limit derived from the noise in the spectrum, that these EWs could be measured to be lower, pushing down the measured Ly α fraction.

Moreover, it is also important to consider the problem of cosmic variance. Even selecting over an area of 0.25 sq. degrees, our sample is clearly limited by small number statistics. As illustrated by Fig. 6, previous samples of luminous $z \sim 6$ LBGs selected over the GOODS fields (the CANDELS imaging in the UDS covers the area of one GOODS field) will include very few, if any, objects as luminous as those in our sample. Again, this simply highlights the point that our sample is exploring a new area of parameter space.

4.2.4 Photometric redshift selection

One potential issue which needs to be addressed is the fact that our original object selection was performed using the Subaru z' -band imaging in the UDS which, for objects at $z \geq 6$, is affected by both IGM absorption and a varying Ly α emission line contribution. As a result, we can probably regard our estimate of 54% for the fraction of luminous $z \simeq 6$ LBGs which display Ly α emission with $\text{EW} \geq 25\text{\AA}$ as an upper limit. The fundamental reason for this is that, due to our original photometric redshift selection our spectroscopic sample is not an entirely random sampling of the parent population satisfying the colour-cut criteria listed previously. In fact, because we targeted objects with the highest probability of being at $z \geq 6$, the location of the Ly α emission line within the selection filter introduces a bias towards preferentially targeting objects with strong Ly α emission. In short, the presence of strong Ly α emission leads to an exaggerated Lyman break and an apparently bluer UV spectral slope, both of which can conspire to produce a more robust photometric redshift solution at $z \geq 6$ than would otherwise be the case.

4.3 An unbiased estimate of the Lyman-alpha fraction using UV continuum selection

Given the complications introduced by selecting our original $z \geq 6$ sample in the Subaru z' -band, we can take advantage of the availability of the NB921 imaging data to investigate the Ly α fraction in a UV-continuum selected sub-sample. In general, for $z < 6.4$ where the narrow-band imaging is clear of the Lyman-break, we expect the narrow-band fluxes to be the same or brighter than the z' -band fluxes for any object with no Ly- α emission (this is reversed if there is strong Ly α emission contributing to the z' -band). A comparison of the z' -band and NB921 photometry for our sample suggests that our original selection limit of $z' \leq 26$ provides a complete sample of objects with $z_{921} \leq 25.7$ (all objects satisfying equations 7 & 8 with $z_{921} \leq 25.7$ also obey $z' \leq 26$). This narrow-band magnitude cut corresponds to an absolute UV magnitude of $M_{UV} = -21.0$ at $z = 6$ and $M_{UV} = -21.1$ at $z = 6.5$ (assuming a flat UV slope in f_ν). At this limit we find 45% of objects (5/11) with Ly α $\text{EW} \geq 25\text{\AA}$, confirming a high fraction of Ly α emitters at $M_{UV} \leq -21.1$.

4.4 A lower limit to the Lyman-alpha fraction

Using our spectroscopic sample it is also possible to estimate a hard lower limit to the Ly α fraction amongst luminous $z \geq 6$ LBGs, if we consider the unlikely scenario in which our $\text{EW} \geq 25\text{\AA}$ Ly α detections are the *only* strong Ly α emitters out of the 19 objects which could have been spectroscopically targeted. Even in this extreme scenario the fraction of galaxies showing Ly α with $\text{EW} \geq 25\text{\AA}$ is $37\% \pm 14\%$ (7/19), where the quoted error is the poisson uncertainty.

However, in reality, this situation is better described by a binomial distribution which predicts that the probability of finding 7 or more galaxies with $\text{EW} \geq 25\text{\AA}$ from a sample of 14 is only $p = 0.01$, if the chance of “success” in each trial (i.e. finding $\text{EW} \geq 25\text{\AA}$) is $p = 0.20$ (as is the case for the most luminous $z \sim 6$ objects in Stark et al. 2011). However,

given the potential for bias, perhaps a more reasonable calculation is to determine the probability of finding 7 or more galaxies with $EW \geq 25\text{\AA}$ from all 19 *potential* spectroscopic targets. This returns a probability of $p = 0.07$, meaning that we are only able to exclude the hypothesis that the true fraction of $EW \geq 25\text{\AA}$ Ly α emitters within our sample is 20% at the $\simeq 93\%$ confidence level.

4.5 Dust free luminous LBGs

Our Ly α fraction results are plotted in Fig. 7 along with the results of Stark et al. (2010, 2011) and Ono et al. (2011). It is clear from this plot that our best estimate of $\simeq 45\%$ for the Ly α fraction amongst luminous LBGs at $z \simeq 6$ is significantly higher than found by Stark et al. (2011) at the same redshift and by Ono et al. (2011) at $z \simeq 7$ (although we note that, before combining their results with other studies taken from the literature, they find a fraction of $\simeq 33\%$). As far as we can tell, this result is not significantly biased by our sample selection and, as can be seen from Fig. 7, is in good agreement with a simple extrapolation of the Ly α fraction derived by Stark et al. (2010) for luminous LBGs at $z = 4$ and $z = 5$.

One possibility is that by sampling the bright end of the $-21.75 < M_{UV} < -20.25$ bin, we are starting to see the effects of targeting the extreme tail of the population of the less-dusty, highly star forming systems. As we move to brighter and brighter objects, the extremely steep slope of the luminosity function would seem to require that samples eventually become dominated by objects with low dust reddening and, presumably, a correspondingly high escape fraction of Ly α photons. Although this scenario would run counter to the observation that, at a given redshift, brighter UV-selected galaxies are generally redder than their low-luminosity counterparts, we note that the median UV slope of our sample is $\langle\beta\rangle = -2.51$. This is bluer than the median value of $\beta = -2.06^{+0.12}_{-0.09}$ for $z \sim 6$, $L > 0.75L^*$ derived by Finkelstein et al. (2011) and the variance-weighted mean value derived at $z \simeq 6.5$ by McLure et al. (2011) of $\langle\beta\rangle = -2.05 \pm 0.09$, although in the absence of deeper near-IR photometry it is difficult to draw any firm conclusions regarding the UV slopes of our sample.

4.6 A UV continuum selected sample

As discussed previously, selecting $z \geq 6$ galaxy samples based on z' -band photometry involves the added complications of varying amounts of IGM absorption and Ly α contamination. In this study, we were able to correct any possible biases by using narrow-band imaging data red-wards of Ly α to define a sample complete to a given depth in the UV continuum. However, to achieve this at higher redshifts it is clearly necessary to perform the primary sample selection in the near-infrared. Within this context, the new Cosmic Assembly Near-infrared Deep Extragalactic Legacy Survey (CANDELS; Koekemoer et al. 2011; Grogin et al. 2011) will supply deep, near-infrared, imaging (5σ depth of $H_{160} \simeq 27$) over a total area of ~ 700 square arcmin. The combination of depth and area provided by CANDELS will allow the Ly α fraction amongst large, unbiased, samples of $z > 7$ LBGs to be studied in the near future.

5 CONCLUSIONS

Targeting a sample of $z \geq 6$ galaxy candidates originally selected using a photometric redshift analysis, we obtained a very high redshift completeness, with 11/14 objects providing robust spectroscopic redshifts from the detection of a Ly α emission line. Comparing the star-formation rate estimates based on UV continuum and Ly α luminosity we find that our sample is consistent with a Ly α escape fraction of $f_{esc}^{Ly\alpha} \simeq 25\%$, in agreement with the recent study of Hayes et al. (2011).

Based on our sample of $L \geq 2L^*$ LBGs at $z \simeq 6$ we derive estimates for the maximum ($54\% \pm 20\%$) and minimum ($37\% \pm 14\%$) fraction of Ly α emitters with $EW \geq 25\text{\AA}$. Testing whether these fractions are biased by our z' -band selection criteria, we use the available NB photometry to calculate the fraction of $EW \geq 25\text{\AA}$ Ly α emitters amongst a complete, UV continuum selected, sub-sample. This calculation returns a fraction of $45\% \pm 15\%$, consistent with our previous estimates.

Our estimate of the $EW \geq 25\text{\AA}$ Ly α emitter fraction in the magnitude range $-21.75 < M_{UV} < -21.25$ is a factor of $\simeq 2$ larger than previous estimates (i.e. $20 \pm 8\%$; Stark et al. 2011). Indeed, we calculate that our sample is inconsistent with a Ly α emitter fraction of 20% at the $\simeq 93\%$ confidence level. However, we also note that our sample explores a higher redshift and luminosity range than previous studies.

In summary, our results suggest that, as the epoch of reionization is approached, it is plausible that the Ly α emitter fraction amongst luminous ($L \geq 2L^*$) LBGs shows a similarly sharp increase to that observed in their lower-luminosity ($L \leq L^*$) counterparts.

ACKNOWLEDGMENTS

The authors would like to acknowledge the anonymous referee for a report which helped to improve the original manuscript. ECL would like to acknowledge financial support from the UK Science and Technology Facilities Council (STFC) and the Leverhulme Trust. RJM would like to acknowledge the funding of the Royal Society via the award of a University Research Fellowship and the Leverhulme Trust via the award of a Philip Leverhulme research prize. JSD acknowledges the support of the Royal Society via a Wolfson Research Merit award, and also the support of the European Research Council via the award of an Advanced Grant. MC acknowledges the award of an STFC Advanced Fellowship. DPS acknowledges support from NASA through Hubble Fellowship grant #HST-HF-51299.01 awarded by the Space Telescope Science Institute, which is operated by the Association of Universities for Research in Astronomy, Inc., for NASA under contract NAS5-26555. HJP, RC, and EB acknowledge the award of an STFC PhD studentships. WGH acknowledges the award of an STFC PDRA. The authors would like to thank the HiZELS team for supplying the Subaru NB921 imaging data and the staff at UKIRT for operating the telescope with such dedication under difficult circumstances.

REFERENCES

- Adelberger K. L., Steidel C. C., Shapley A. E., Pettini M., 2003, *ApJ*, 584, 45
- Ando M., Ohta K., Iwata I., Akiyama M., Aoki K., Tamura N., 2006, *ApJ*, 645, L9
- Bouwens R. J., Illingworth G. D., Franx M., Ford H., 2007, *ApJ*, 670, 928
- Bouwens R. J., Illingworth G. D., Oesch P. A., Labbé I., Trenti M., van Dokkum P., Franx M., Stiavelli M. et al., 2011, *ApJ*, 737, 90
- Bouwens R. J., Illingworth G. D., Oesch P. A., Franx M., Labbé I., Trenti M., van Dokkum P., Carollo C. M. et al., 2011, eprint arXiv:1109.0994
- Bouwens R. J., Illingworth G. D., Oesch P. A., Stiavelli M., van Dokkum P., Trenti M., Magee D., Labbé I. et al., 2010, *ApJ*, 709, L133
- Bouwens R. J., Illingworth G. D., Oesch P. A., Trenti M., Stiavelli M., Carollo C. M., Franx M., van Dokkum P. G., Labbé I., Magee D., 2010, *ApJ*, 708, L69
- Bruzual G., Charlot S., 2003, *MNRAS*, 344, 1000
- Calzetti D., Armus L., Bohlin R. C., Kinney A. L., Koornneef J., StorchiBergmann T., 2000, *ApJ*, 533, 682
- Casali M., Adamson A., Alves de Oliveira C., Almaini O., Burch K., Chuter T., Elliot J., Folger M. et al., 2007, *A&A*, 467, 777
- Chabrier G., 2003, *Publications of the Astronomical Society of the Pacific*, 115, 763
- Dayal P., Ferrara A., 2011, eprint arXiv:1109.0297
- Dijkstra M., Mesinger A., Wyithe J. S. B., 2011, *Monthly Notices of the Royal Astronomical Society*, 414, 2139
- Finkelstein S. L., Papovich C., Giallisco M., Reddy N. A., Ferguson H. C., Koekemoer A. M., Dickinson M., 2010, *ApJ*, 719, 1250
- Finkelstein S. L., Papovich C., Salmon B., Finlator K., Dickinson M., Ferguson H. C., Giallisco M., Koekemoer A. M. et al., 2011, eprint arXiv:1110.3785
- Fontana A., Vanzella E., Pentericci L., Castellano M., Giallisco M., Grazian A., Boutsia K., Cristiani S. et al., 2010, *ApJ*, 725, L205
- Furusawa H., Kosugi G., Akiyama M., Takata T., Sekiguchi K., Tanaka I., Iwata I., Kajisawa M. et al., 2008, *ApJS*, 176, 1
- Forero-Romero J. E., Yepes G., Gottloeber S., Prada F., 2011, eprint arXiv:1109.0228
- Grogin N. A., Kocevski D. D., Faber S. M., Ferguson H. C., Koekemoer A. M., Riess A. G., Acquaviva V., Alexander D. M. et al., 2011, eprint arXiv:1105.3753
- Hainline K. N., Shapley A. E., Greene J. E., Steidel C. C., 2011, *ApJ*, 733, 31
- Hayes M., Schaerer D., Östlin G., Mas-Hesse J. M., Atek H., Kunth D., 2011, *ApJ*, 730, 8
- Hewett P. C., Warren S. J., Leggett S. K., Hodgkin S. T., 2006, *MNRAS*, 367, 454
- Hu E. M., Cowie L. L., McMahon R. G., 1999, *The High-Redshift Universe: Galaxy Formation and Evolution at High Redshift*, 193
- Ilbert O., Arnouts S., McCracken H. J., Bolzonella M., Bertin E., Le Fèvre O., Mellier Y., Zamorani G. et al., 2006, *A&A*, 457, 841
- Jiang L., Egami E., Kashikawa N., Walth G., Matsuda Y., Shimasaku K., Nagao T., Ota K., Ouchi M., 2011, eprint arXiv:1109.0023
- Koekemoer A. M., Faber S. M., Ferguson H. C., Grogin N. A., Kocevski D. D., Koo D. C., Lai K., Lotz J. M. et al., 2011, eprint arXiv:1105.3754
- Lawrence A., Warren S. J., Almaini O., Edge A. C., Hamblly N. C., Jameson R. F., Lucas P., Casali M. et al., 2007, *MNRAS*, 379, 1599
- McLure R. J., Cirasuolo M., Dunlop J. S., Foucaud S., Almaini O., 2009, *MNRAS*, 395, 2196
- McLure R. J., Dunlop J. S., Cirasuolo M., Koekemoer A. M., Sabbi E., Stark D. P., Targett T. A., Ellis R. S., 2010, *MNRAS*, 403, 960
- McLure R. J., Dunlop J. S., de Ravel L., Cirasuolo M., Ellis R. S., Schenker M., Robertson B. E., Koekemoer A. M. et al., 2011, eprint arXiv:1102.4881
- McLure R. J., Jarvis M. J., Targett T. A., Dunlop J. S., Best P. N., 2006, *MNRAS*, 368, 1395
- Madau P., 1995, *ApJ*, 441, 18
- Madau P., Pozzetti L., Dickinson M., 1998, *ApJ*, 498, 106
- Nilsson K. K., Tapken C., Møller P., Freudling W., Fynbo J. P. U., Meisenheimer K., Laursen P., Östlin G., 2009, *A&A*, 498, 13
- Oke J. B., Gunn J. E., 1983, *ApJ*, 266, 713
- Ono Y., Ouchi M., Mobasher B., Dickinson M., Penner K., Shimasaku K., Weiner B. J., Kartaltepe J. S. et al., 2011, eprint arXiv:1107.3159
- Ouchi M., Shimasaku K., Akiyama M., Simpson C., Saito T., Ueda Y., Furusawa H., Sekiguchi K. et al., 2008, *ApJS*, 176, 301
- Ouchi M., Mobasher B., Shimasaku K., Ferguson H. C., Fall S. M., Ono Y., Kashikawa N., Morokuma T., Nakajima K., Okamura S., Dickinson M., Giallisco M., Ohta K., 2009, *ApJ*, 706, 1136
- Ouchi M., Shimasaku K., Furusawa H., Saito T., Yoshida M., Akiyama M., Ono Y., Yamada T. et al., 2010, *ApJ*, 723, 869
- Pentericci L., Fontana A., Vanzella E., Castellano M., Grazian A., Dijkstra M., Boutsia K., Cristiani S. et al., 2011, eprint arXiv:1107.1376
- Reddy N. A., Steidel C. C., Pettini M., Adelberger K. L., Shapley A. E., Erb D. K., Dickinson M., 2008, *ApJS*, 175, 48
- Schenker M. A., Stark D. P., Ellis R. S., Robertson B. E., Dunlop J. S., McLure R. J., Kneib J. P., Richard J., 2011, eprint arXiv:1107.1261
- Sekiguchi K., Akiyama M., Furusawa H., Simpson C., Takata T., Ueda Y., Watson M. W., The Sxds Team 2005, *Multiwavelength Mapping of Galaxy Formation and Evolution. ESO Astrophysics Symposia*, Springer-Verlag, Berlin/Heidelberg
- Shapley A. E., Steidel C. C., Pettini M., Adelberger K. L., 2003, *ApJ*, 588, 65
- Shimasaku K., Kashikawa N., Doi M., Ly C., Malkan M. A., Matsuda Y., Ouchi M., Hayashino T. et al., 2006, *PASJ*, pp 313–334
- Sobral D., Best P., Matsuda Y., Smail I., Geach J., Cirasuolo M., 2011, eprint arXiv:1109.1830
- Stark D. P., Ellis R. S., Chiu K., Ouchi M., Bunker A., 2010, *MNRAS*, 408, 1628
- Stark D. P., Ellis R. S., Ouchi M., 2011, *ApJ*, 728, L2
- Steidel C. C., Hunt M. P., Shapley A. E., Adelberger K. L., Pettini M., Dickinson M., Giallisco M., 2002, *ApJ*, 576,

653

- Steidel C. C., Pettini M., Hamilton D., 1995, *The Astronomical Journal*, 110, 2519
- Vanzella E., Giavalisco M., Dickinson M., Cristiani S., Nonino M., Kuntschner H., Popesso P., Rosati P. et al., 2009, *ApJ* 695, 1163
- Vanzella E., Pentericci L., Fontana A., Grazian A., Castellano M., Boutsia K., Cristiani S. et al., 2011, *ApJ*, 730, L35
- Willott C. J., Delorme P., Reyl   C., Albert L., Bergeron J., Crampton D., Delfosse X., Forveille T. et al., 2009, *The Astronomical Journal*, 137, 3541
- Willott C. J., Delorme P., Reyl   C., Albert L., Bergeron J., Crampton D., Delfosse X., Forveille T. et al., 2010, *The Astronomical Journal*, 139, 906
- Yoshida M., Shimasaku K., Kashikawa N., Ouchi M., Okamura S., Ajiki M., Akiyama M., Ando H. et al., 2006, *ApJ*, 653, 988